SAND2019-12914C

Launching Digital Image Correlation as an Experimental Modal Analysis Capability

Bryan Witt, Dan Rohe
Sandia National Laboratories*
P.O. Box 5800 - MS0557
Albuquerque, NM, 87185
blwitt@sandia.gov, dprohe@sandia.gov

ABSTRACT

Digital image correlation (DIC) is an established test technique in several fields including quasi-static strain measurements. Recently there has been growing interest in using DIC to measure structural dynamic response and even extract modal parameters from that information. While high-speed cameras have become more ubiquitous, there are no commercial end-to-end packages for modal analysis based on image data, particularly when combined with traditional data acquisition systems. As such, the practitioner is left to develop several key data processing capabilities, hardware interface equipment, and testing practices themselves. This work highlights several practical aspects that have been encountered in attempting to launch DIC as a viable modal testing capability in a laboratory environment.

Keywords: Digital Image Correlation, High-Speed Imaging, Photogrammetry, Modal, Practical Application

1 INTRODUCTION

The use of high-speed stereo photogrammetry, specifically stereo digital image correlation (DIC), to perform structural dynamic measurements is currently gaining interest. While DIC is well established for measurements such as quasi-static strain or large-scale motion tracking, it is far less commonly studied for applications where low amplitude (sub millimeter) and high frequency (>500 Hz) measurements are required, such as experimental modal analysis (EMA). The application of DIC to modal testing is not new and has been demonstrated to work well for low-frequency and/or high-amplitude applications by several authors, e.g. [1, 2, 3]. The primary reason DIC has been limited in these applications is the fact that the measured displacements diminish as a square of the frequency, meaning that the displacements typically incurred by modal excitation fall below the noise floor of DIC at relatively low frequencies. This observation is relative since the measurement resolution, and thus what constitutes a "small" displacement, of a DIC setup is dependent of the field of view (FOV). With an appropriate test setup and employment of noise mitigation techniques, DIC-based EMA tests can be successfully conducted for very small displacements and high frequencies. Efforts are underway to establish high-speed stereo DIC as a generalized modal testing capability in the laboratory to supplement other measurement techniques. A step-by-step guide to conducting DIC tests is outside the scope of this work, and the reader is referred instead to such resources as the best-practices guide produced by the International Digital Image Correlation Society [4]. This work is intended to offer several practical aspects that have been encountered while implementing DIC specifically for modal testing. Aspects of test planning and setup are discussed first, followed by comments on executing modal DIC tests. Most of this work focuses on post-processing optical data for modal analysis and cursory techniques for noise mitigation, as these are the least documented in literature.

---

* Sandia National Laboratories is a multimission laboratory managed and operated by National Technology and Engineering Solutions of Sandia, LLC., a wholly owned subsidiary of Honeywell International, Inc., for the U.S. Department of Energy's National Nuclear Security Administration under contract DE-NA-0003525.

2 TEST PLANNING

Test planning begins by defining the ultimate goals of a test. While it is not uncommon in modal DIC work to approximate natural frequencies from peaks in response spectra and shapes from their corresponding operational deflection shapes (ODS), the goal in this work is to extract natural frequencies, damping ratios, and mass-normalized mode shapes using a modal parameter estimation algorithm of choice. ODS are useful in many applications, but actual modal parameters are necessary for a quantitative validation of analytical models. Since scaled mode shapes are desired, input forces and drive point responses are required. While the drive point response could in many cases come from an optical measurement, the excitation force cannot. This necessitates the need to combine DIC measurements with a traditional data acquisition system (DAS). While this adds complexity, the overall time savings in using optical measurements can outweigh the upfront time-cost of setting up both the DIC system and a DAS which is recording a minimal set of force and acceleration sensors. Further, the use of a drive point accelerometer (at a minimum) is beneficial beyond its use in scaling mode shapes for the following reasons:

- The high signal-to-noise (SNR) signal is helpful in identifying frequencies of interest that are below the camera noise floor [5]
- The accelerometer data can be used to help quickly specify DAS settings such as window length to prevent leakage
- If sampled beyond the camera frame rate, the accelerometer can provide an indication if aliasing may be present in the optical data. This is a concern for DIC which has no practical means of performing anti-alias filtering that is found on most modern DAS.

The use of both systems will need to be considered in the test planning phase. In many cases, the use of supplemental accelerometers in areas that are not in the line of sight of the DIC system will be necessary, e.g. for internal measurement locations. While supplemental accelerometers can be used to measure locations that are not in one FOV, it should be kept in mind that data sets in multiple FOV can be set up and easily combined in post-processing. This is predicated on the practice of transforming all optically measured data into the test object's coordinate system, as will be discussed in Section 5.1. For example, the front, sides, and back of a test object can be scanned to generate full mode shapes of a test object.

The DIC measurement quantity of interest is displacement, which decreases in amplitude with the square of frequency. Therefore, the noise floor of the DIC system will be the limiting factor when extracting higher frequency modes. As such, a major consideration in the planning effort should involve estimating the pixels of displacement that can be expected for a given test setup. This is a function of the test article's modes, the excitation used, the camera resolution, and the field of view. Experience to date has shown that peak displacements on the order of 0.1 pixel are generally sufficient to extract meaningful modal data. Estimating expected pixels of displacement is not a straightforward task, and tools to help with this scoping analysis are actively being developed. The use of virtual DIC [6] has great potential for this type of survey, although it requires a finite element model (FEM) and image rendering software, such as Blender. An example of an actual test image and its corresponding Blender rendering is shown in Fig. 1. Without careful planning, it is possible that a test will be conducted for which no meaningful data can be extracted, and this will only become apparent after considerable time and effort have been expended and large quantities of data have been generated.

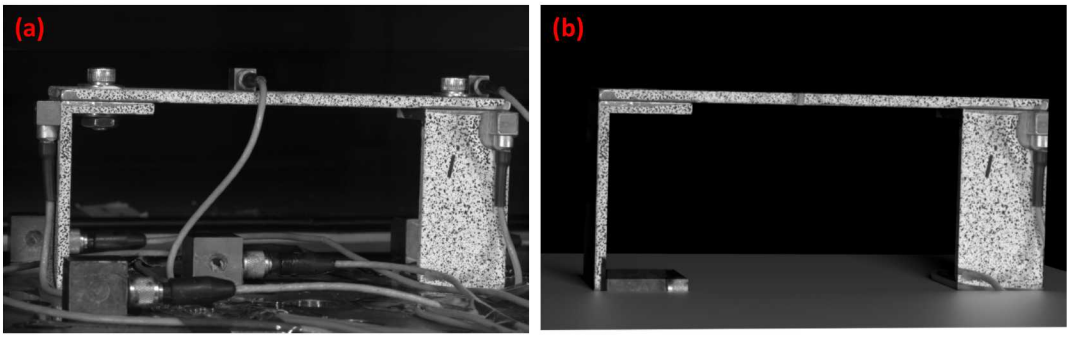

Fig. 1 Using virtual DIC as a test planning tool, (a) actual test image (b) virtual rendering

A final planning consideration, that is obvious but sometimes overlooked, is the data storage requirement. Terabytes of image data are easily generated per test, but not so easily transferred, processed, and stored. It is wise to determine a procedure or requirements for long-term image storage at the outset of establishing DIC as a modal testing tool.

3 TEST SETUP

The first stereo-DIC test setup decision is the selection of cameras. Several suitable commercial cameras are available; the examples presented in this work were taken with Vision Research Phantom v2640 cameras. These have a maximum frame

rate of 6,600 fps at a full resolution of 2048x1920 pixels, which is adequate to capture a useful bandwidth of ~3 kHz. Three modal-specific comments are offered for camera selection:

- *There is no substitution for pixels.* This is the first and most logical method for increasing DIC resolution (pixels/unit length) and thereby reducing optical data noise, even though this results in larger data files.
- *Extreme frame rates are not necessarily required*. Satisfying the Nyquist criterion for frequency domain analysis (2x highest frequency of interest) is adequate for general modal applications. Care must be taken that the test object is not responding at frequencies beyond the Nyquist, which will introduce aliasing. This can largely be managed by not providing excitation at frequencies beyond the Nyquist.
- *Onboard non-volatile memory is extremely useful*. For example, the Vision Research cameras used have a CineMag option which allows the camera's volatile memory to be rapidly offloaded to a removable non-volatile disk. This greatly reduces the time between test runs and minimizes the opportunities for inadvertent test article changes (bungee cords sagging, cameras bumped, etc.). The larger memory size on the disks also increases the number of data sets that may be collected before time consuming data transfers must be conducted.

Maximizing the pixels spread across the test object's areas of interest (AOI) is of paramount importance. For a given camera resolution, this is controlled by carefully setting the FOV such that the AOI are maximized but will also remain in the image frame and stay in focus during excitation. For these fine adjustments, a camera stand that is both rigid and easily adjustable is necessary. Experience to date has shown that the below are desirable attributes for a modal DIC camera stand:

- Rigid bar on which both cameras mount
- Easy adjustment of camera body translation and stereo angle
- Easy adjustment of camera bar height and rotation
- Rolling chassis for stand transport and placement
- Chassis screw jacks for anchoring and leveling

An example stand configuration is shown in Fig. 2. The frame is constructed from 95 mm optical railing for rigidity. The camera baseline distance and stereo angles are easily adjusted using optical railing clamps to which camera swivel mounts are attached. The vertical height of the camera rail is adjusted via a scissor mechanism that also provides lateral stability. The camera rail is mounted on two angle joints that together keep the bar fixed but allow a rotation angle to be set. The chassis also has swivel casters and screw jacks. Several variations of similar camera stands have been used and are often configured to best suit a specific test.

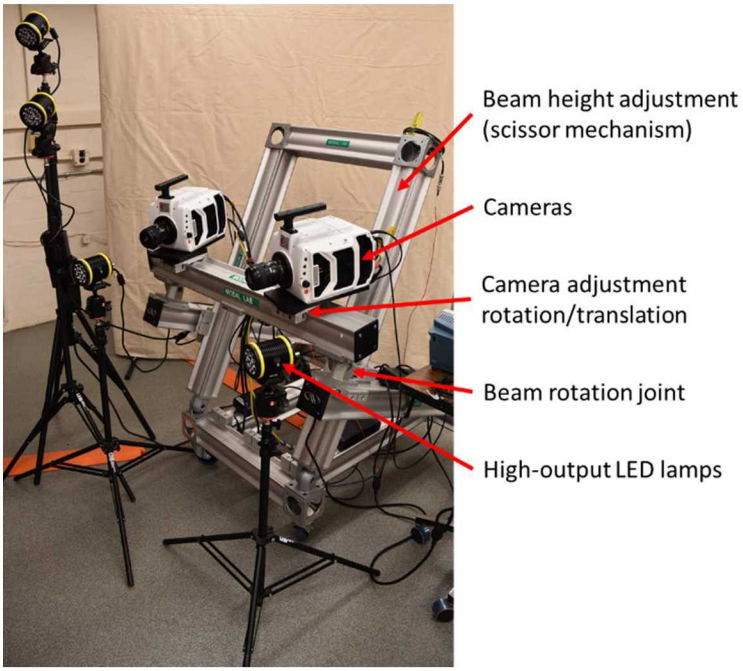

Fig. 2 Example of an adjustable high-speed stereo camera mounting stand

DIC requires the test article's AOI be prepared with some kind of contrast field, typically a speckle pattern. Unlike a static pull-to-failure test for strain analysis, modal testing has the benefit of only incurring small continuous displacements. As a result, speckle patterns can be applied to the test article in several ways, including via printable adhesive paper. Not only is

this quick to apply and remove relative to painting the test object, a customized speckle pattern can be numerically generated that is optimized for the test at hand. Implementing a speckle pattern generator that can randomize speckle size and offset (jitter) distributions is easily accomplished in tools such as Matlab or Python, examples of which are shown in Fig. 3. Readily available laser printer shipping labels have been found to be an acceptable medium for creating such speckle pattern appliqués.

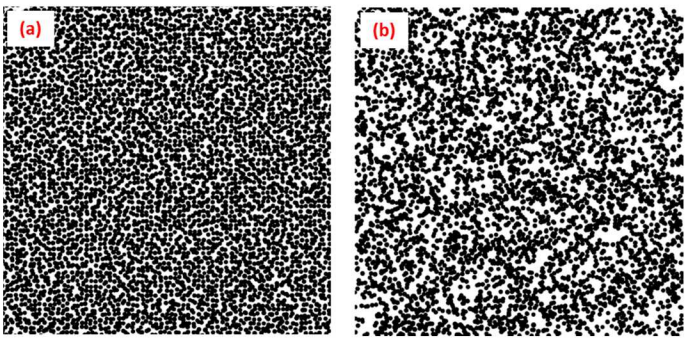

Fig. 3 Examples of numerically generated speckle patterns (a) jitter random (b) pure random

Following a stereo calibration, it is general DIC practice to collect static images for noise floor estimation as well as to establish an undeformed reference image. Averaging the static images taken to generate a cleaner reference image is beneficial. One practical consideration for modal testing with an electrodynamic shaker is to take the static images with the shaker attached to the test object and powered on. This should be done as soon as possible before conducting the actual modal test. When power is applied to the shaker, the armature will move to its stable position. If the static images are taken prior to this, the undeformed reference image will have a (potentially large) displacement offset relative to the series of deformed images that will subsequently be collected for DIC analysis.

For many general modal tests, a separate DAS will be used to collect the load cell and accelerometer data that will be combined with the optical measurements. While the sample rate of the camera can be arbitrarily specified, many modal DAS systems have preferred sample rate settings that may not align with the desired camera sample rate. Simply sampling faster with the cameras to compensate will result in additional data storage and processing time requirements beyond what are necessary. Instead, the DAS can be oversampled relative to the cameras and subsequently resampled later. Care should be taken to account for aliasing in down-sampling the data, using something similar to Matlab's *resample* function. As mentioned above, oversampling the DAS also provides a means for determining if there are potential aliasing issues in the optical data (which has no anti-aliasing filter).

The DAS and cameras need to be triggered simultaneously in order to roughly synchronize the optical and load cell/accelerometer data. For shaker excitation, a momentary closed-contact switch that is connected to both camera trigger ports and also an input channel of the DAS works well. For impact excitation, such as a modal hammer, a secondary device is necessary to generate a transistor-transistor logic (TTL) signal once the force signal crosses a threshold. This can be a simple device; for example, an Arduino Uno microcontroller was programmed to perform this function, with the signal conditioning for the load cell being provided by a PCB 480C02 (see Fig. 4).

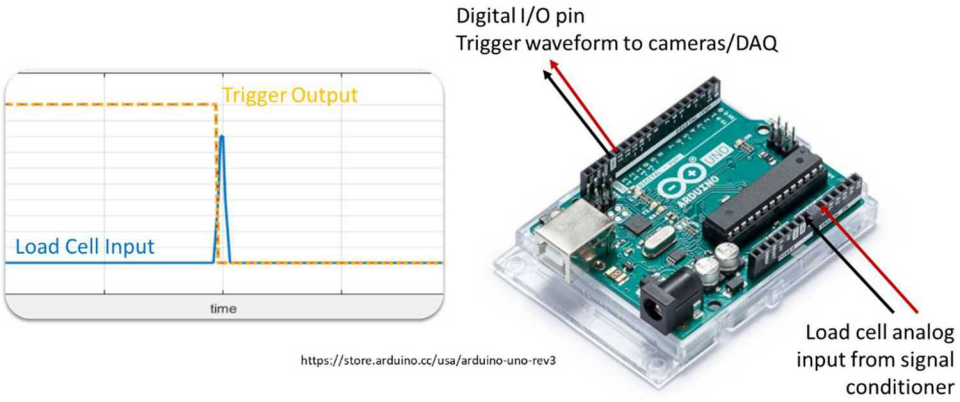

Fig. 4 Arduino as a trigger system for hammer impacts

Triggering the cameras and the DAS from a common source does not actually synchronize them; the degree to which they are off is a function of the settings of either system. Both systems will begin collecting data on the sample following the trigger event. This is depicted in Fig. 5. Since there is no synchronization between either system's sampling clock, there is no expectation that they should sample at the same instant in time. A constant time delay that is likely not an integer of either system's time step, Δt, will exist between the camera and the DAS data sets (the image frame synchronization between cameras can be set on the order of 10 nanoseconds and is considered concurrent). The time delay between the DAS and cameras will be corrected for in post processing, as described in Section 5.1 below.

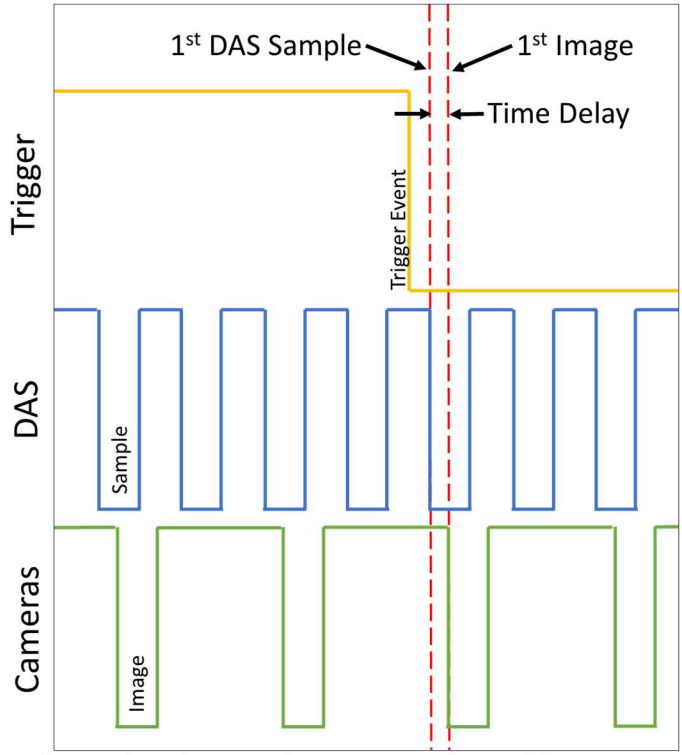

Fig. 5 Triggering and time delay between DAS and cameras

Some cameras support synchronization with specific external DAS products. These supported DASs typically have a limited channel count, but a split signal between them and a higher count modal DAS could be used to subsequently synchronize all systems together. For practitioners that have existing DASs, simply correcting the time delay in post-processing is a practical solution.

4 TEST EXECUTION

The method of mechanical excitation chosen for a DIC modal test has a large impact on data collection and post-processing requirements. Electromechanical shakers have been found to be preferable over modal impact hammers for the following reasons:

- Impact hammers are more difficult to trigger both the DAS and cameras from (refer to Section 3 above), generally requiring some additional hardware to create an appropriate trigger signal at impact.
- Impact excitation tends to require many averages to produce clean frequency response functions (FRFs), meaning that many sets of images are required.
- A new undeformed reference image may be needed between averages, as the test object will not return to the exact reference orientation after each impact. Extreme offsets may cause correlation issues while small offsets will result in a static displacement bias which can be removed in post-processing to prevent low frequency artifacts in the FRF.
- Hammer impacts can result in large rigid body motions which can cause several issues: correlation difficulties, test object leaving the FOV, and/or loss of focus in AOI due to dept of field.
- It can be difficult to control the frequency range of excitation using a modal hammer. This is more of a concern with DIC tests than traditional modal methods because anti-aliasing is difficult to implement for image data; efforts must be made to keep the excitation frequency range below the imaging system's bandwidth.

These issues are surmountable but should be accounted for in test execution if hammer testing is employed.

Shaker excitation helps with several of the aforementioned issues such as triggering, limiting large rigid body motions and controlling the excitation bandwidth to manage aliasing. The type of shaker excitation is an important consideration as well. Pure random excitation generally requires many averages to generate clean FRFs [7], meaning that a large number of images will be required, driving long image transfer and post-processing times. Windowing and overlapping the data in the calculation of the FRFs will help with the total number of images required. Burst random testing may require fewer averages, but the entirety of each averaging frame must be processed as overlapping is not an option. Similarly, sine sweeps/dwells can produce cleaner FRFs at target frequencies but at the cost of long test times (many images) and/or *a priori* knowledge of the structure's resonance frequencies. It is noted that the presence of the drive point and any supplemental accelerometers can be used to identify the resonance frequencies of interest in-test, providing the required *a priori* information for successful sine dwell/sweep testing.

Pseudorandom excitation has been found to have many benefits for DIC-based modal testing. These signal types typically require fewer averages to produce clean FRFs [7], greatly reducing the number of images that must be dealt with. Further, because the signal is deterministic, image averaging may be used which has the combined effect of reducing random image noise and collapsing the number of image frames that DIC is performed on by a factor equal to the number of averages. Fig. 6 depicts the image averaging process. Because pseudorandom is a deterministic signal, corresponding time steps across each averaging frame should result in the same structural response of the test article (provided the structural response has reached steady state and the cameras are not moving). Hence, corresponding images (i.e. time steps) can be averaged, pixel by pixel, across each averaging frame. This has the same noise reduction effect as performing averaging of the FRFs, as is typically done in a traditional modal test, with the additional benefit of reducing the number of images that must be processed through DIC. For example, if 20,480 images (per camera) were collected over 10 averaging frames, there would only be 2,048 averaged images to process through DIC. The actual time savings will vary based on computational equipment, software and DIC settings used, but the authors experience has found this to be the difference in hours vs minutes to perform the correlation.

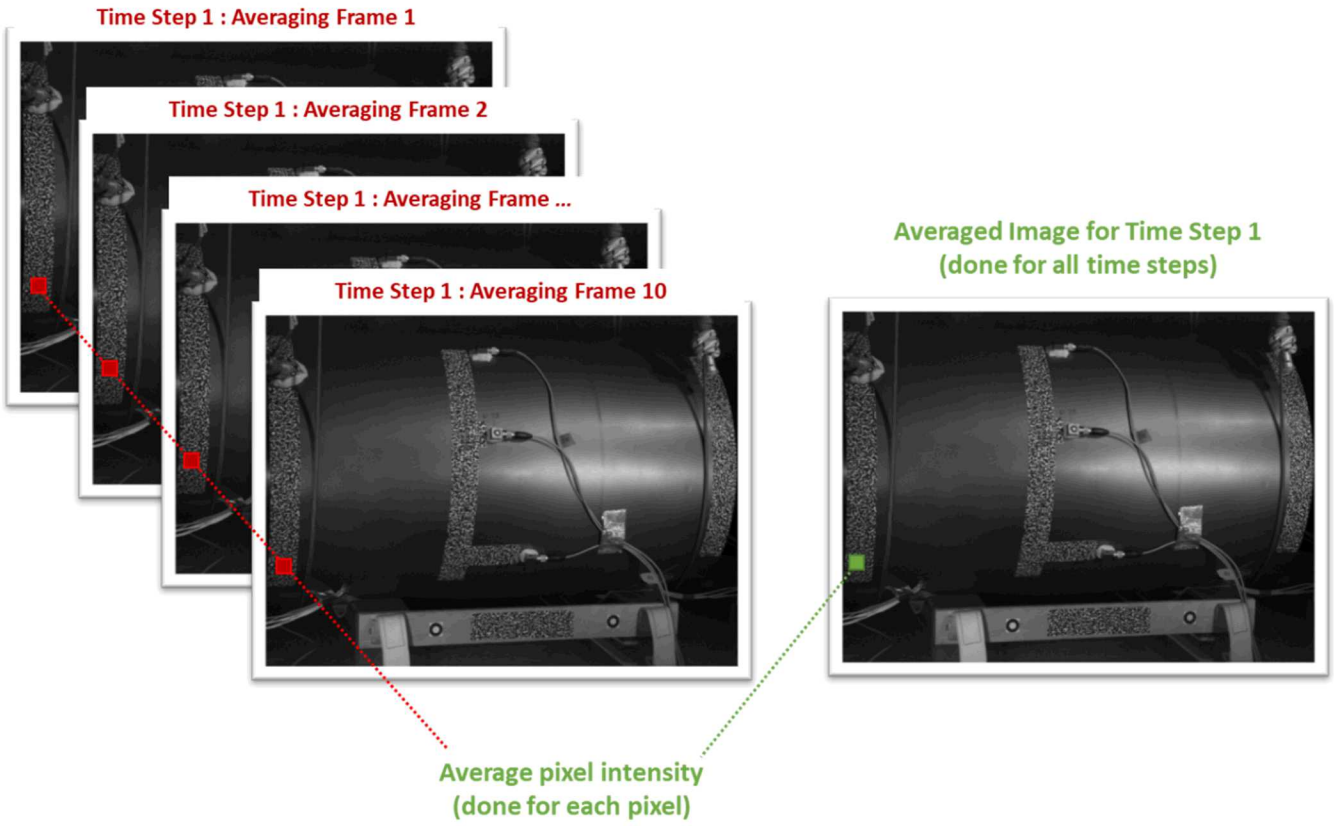

Fig. 6 Image averaging process

Pseudorandom signals are also easily shaped. One technique that has been examined is the use of a ramped-banded pseudorandom signal, where the input signal amplitudes are binned around frequencies of interest (determined beforehand from the drive point accelerometer) and also ramped up at higher frequencies. The impetus was based on attempting to minimize driving the structure between resonances where displacements are small and noise is high while also favoring the higher frequency range where the DIC system noise floor tends to dominate. To demonstrate, three tests were performed on the same aluminum cylindrical structure shown in Fig. 6 using pseudorandom excitation spectra that were (1) flat-broadband, (2) flat-banded, and (3) ramped-banded. The resulting FRFs were used to compute complex mode indicator functions (CMIF) [8], which provide a summary view of all measured FRFs. Peaks in the CMIF indicate the presence of excited, and observable, modes. Below 600 Hz, all modes were easily observed and extracted with all three methods. However, the modes near 1,000 and 1,750 Hz were only directly observable in the FRFs when the ramped excitation method was used, indicating a clear increase in the signal-to-noise ratio at higher frequencies (see Fig. 7). The corresponding mode shape near 1750 Hz for each of the three excitation methods is shown in Fig. 8. Note that these shapes are from combined accelerometer and optical subset data, with the three radial stripes along the external of the cylinder corresponding to the optically measured data. In this particular shape, the cylinder does not move (FEM shape plotted for reference) and the subset DOF should lie flat; deviations from the FEM surface are due to noise. The flat-broadband and flat-banded shapes have a similar level of noise in the optical subset DOF, indicating that banding was not particularly helpful in this case. However, the ramped-banded shape shows a marked decrease in noise which was observed in all shapes, indicating that ramping the input as a function of frequency was beneficial. This particular mode highlights a challenge with using DIC for modal analysis: measurements taken at locations that are at, or near, nodal points in certain shapes will demonstrate a high level of noise in that shape due to the small displacements. The same node may have excellent results for another mode at which it is more active and the displacements are larger.

Another effective excitation technique is to apply a flat-force input spectrum, versus the typical flat-voltage input. This is accomplished by applying a flat-voltage input, measuring the input voltage and resulting input force, creating the voltage-to-force transfer function, and finally calculating the resulting input voltage profile that will result in a flat-force spectrum. This method generates input spectra that will be limited by the shaker amplifier quite quickly. This is due to the system working harder to push the system at resonance. The tradeoff is more excitation at the frequencies of interest, potentially driving their responses further above (or out of) the noise floor.

A final note for test execution is to ensure time history data are collected for the DAS (not just spectral quantities). It is not recommended to combine FRFs that were computed from DAS and camera data independently. Once camera images are processed to time histories and combined with the accelerometer and force channels, all data can then be processed to the frequency domain using the exact same methods and parameters.

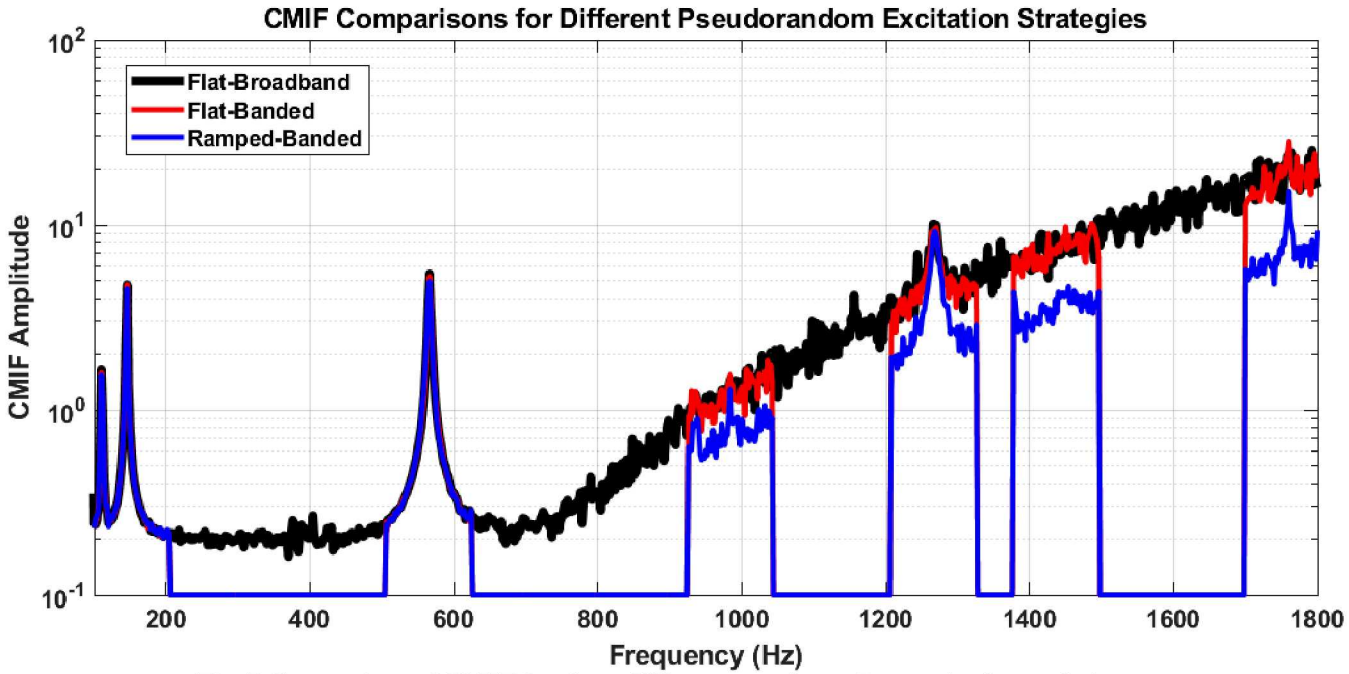

Fig. 7 Comparison of CMIF for three different pseudorandom excitation techniques

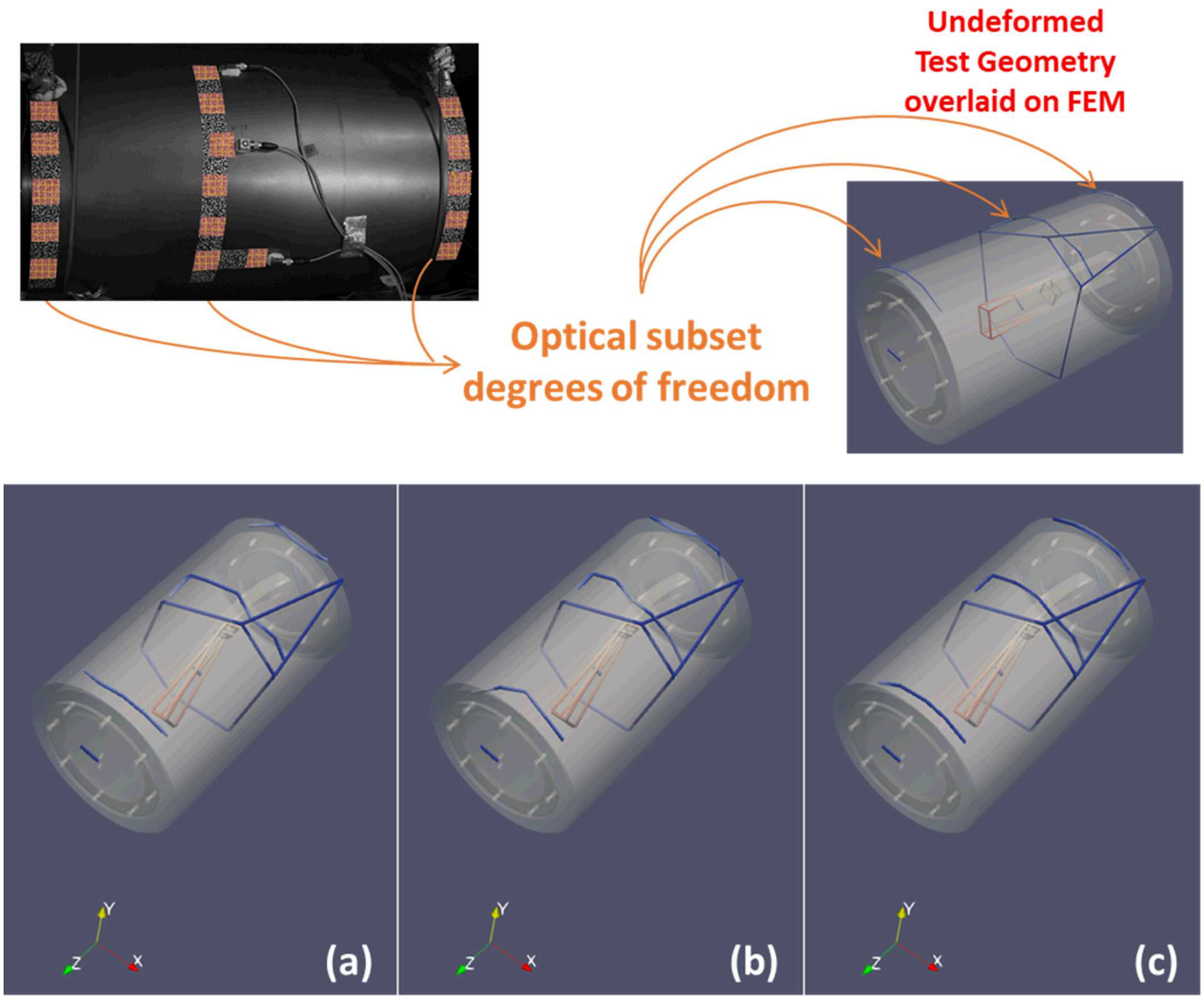

Fig. 8 Comparison of the mode at ~1750 Hz for (a) flat-broadband (b) flat-banded (c) ramped-banded pseudorandom excitation (measured data are wireframes plotted on top of FEM result)

5 POST-PROCESSING

There is currently no commercial end-to-end software for post-processing of combined optical and accelerometer/force transducers for EMA, nor is there comprehensive literature on a practical implementation of such data processing. This section outlines the authors' current practices with the acknowledgement that there are many possible implementations and it is fully expected to change with experience and time.

If image averaging will be implemented, it is done prior to any other data processing. Refer to Section 4 above for details. Once a final set of images are ready for DIC analysis, there are several suitable commercial codes available as well as detailed literature on implementing one's own DIC code [9]. The reader is again referred to the Good Practices Guide [4] for detailed information on how to best perform DIC analysis. One modal-specific comment is offered: large subsets are generally beneficial for modal applications due to the low displacement gradients in the mode shapes of many structures. Larger subsets have the benefit of reducing variance noise, however pattern induced bias and shape function undermatching (particularly for large stereo angles) should be considered when making these decisions.

5.1 DIC Output

DIC output data will require reformatting and further processing to be useful for EMA purposes. First, the DIC output data may be formatted in a matrix form, one per time step (image pair). In such cases, the data for each time step should be flattened and concatenated to create time history vectors for each subset for all subsequent data processing.

Second, correlation issues can cause certain subsets to drop out in different time steps. Interpolation methods can be used to attempt data corrections, however in our current implementation, any subsets with missing time steps are automatically removed entirely as suspect data. This highlights areas where attention may be needed for better data quality (patterning, lighting, or focusing issues for example).

The fundamental measurements from stereo-DIC analysis are the 3D coordinates of each subset for each time step. Most DIC codes will also compute displacements from the reference image automatically. If this is not the case, the user will need to perform this step. At this point, consistency of units between the DAS and optical displacement data is checked and converted as necessary. For example, if the DAS recorded accelerometer and load cell data in Imperial units and the camera data are Metric (based on how the calibration target parameters were defined), a choice must be made, and one set converted to match the other.

Stereo-DIC analysis will produce data in the camera rig coordinate system (CS), which is not particularly useful for model comparisons or combining multi-FOV data sets. A 3D-3D rigid transformation is desired to take the resulting displacement data out of the camera rig coordinate system and into the world, or finite element model CS as shown by the transformation in the center of Fig. 9. This is accomplished using a least-squared rigid motion (LSRM) transformation via a singular value decomposition algorithm [10]. The algorithm requires that a minimum of three points be identified for which the coordinates are known in both systems (rig, and world) and returns the associated rotation matrix **R** and translation vector ***t*** such that:

$$\begin{bmatrix} x \\ y \\ z \end{bmatrix}_{world} = \boldsymbol{R} \begin{bmatrix} x \\ y \\ z \end{bmatrix}_{rig} + \begin{bmatrix} t_x \\ t_y \\ t_z \end{bmatrix} \tag{1}$$

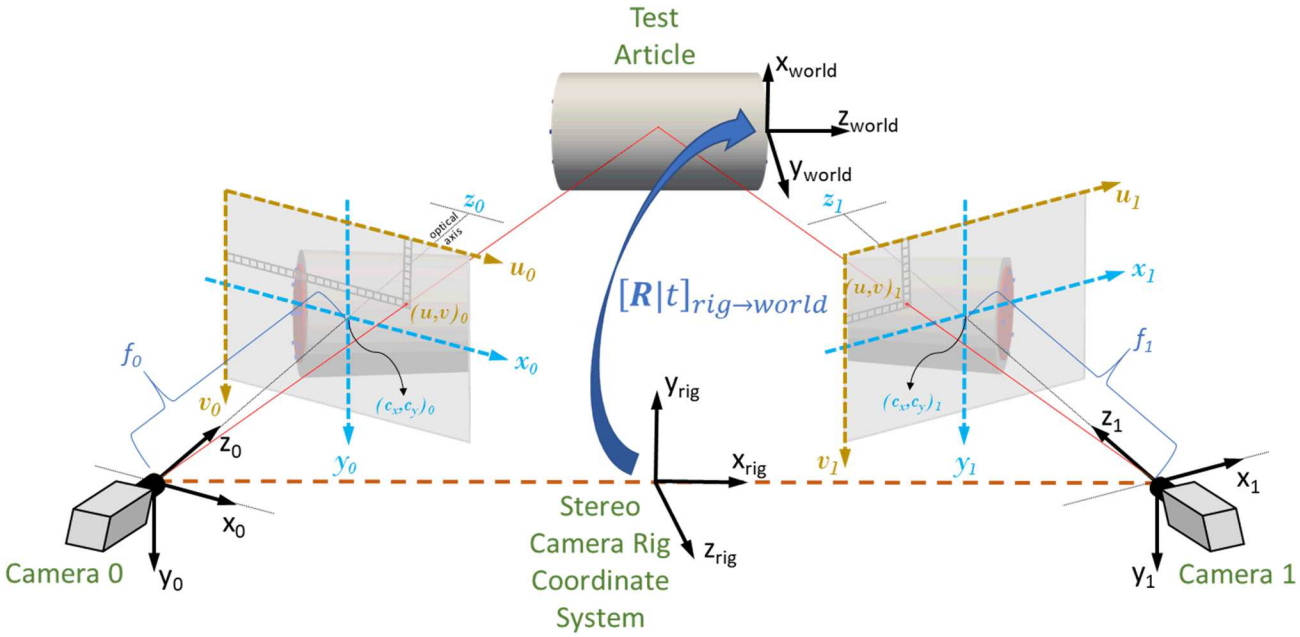

Fig. 9 Camera, camera rig, image plane, and world coordinate systems

The camera rig coordinates can be exported from the DIC software by placing markers at the selected transform points in the reference stereo images. The use of fiducial markers such as contrasting concentric circles (CCC) aids in the easy and

repeatable selection of transformation points (see

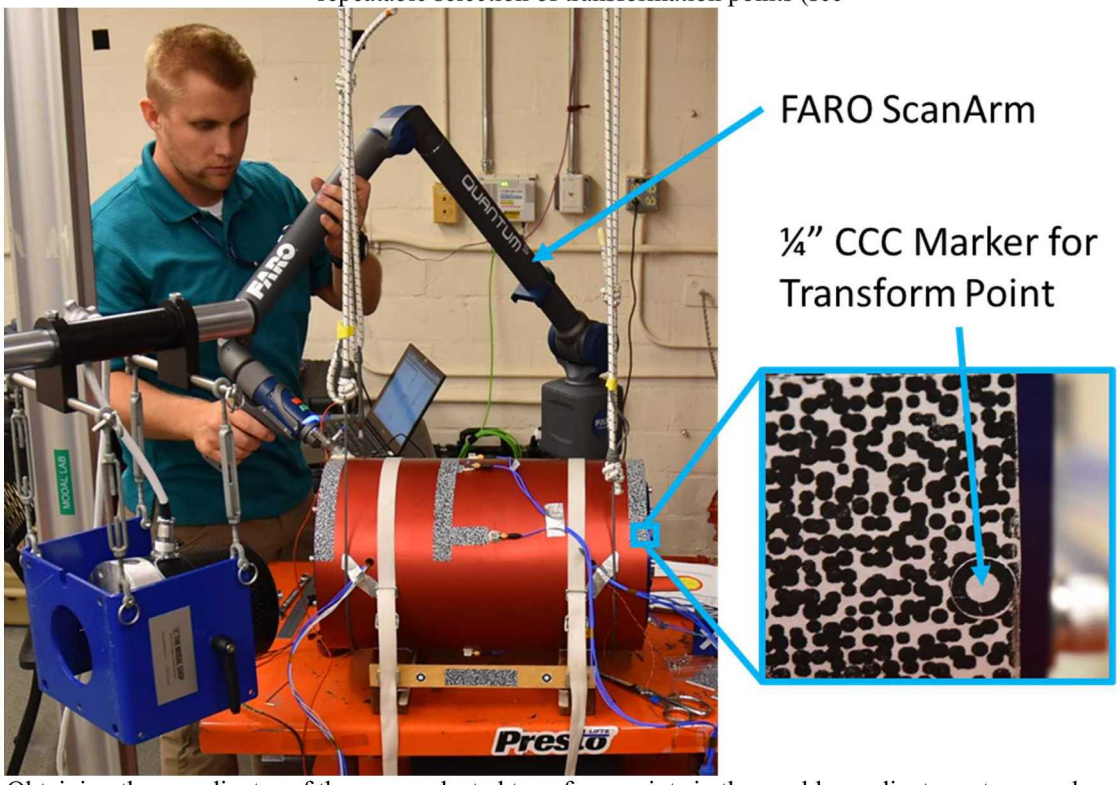

Fig. 10). Obtaining the coordinates of the same selected transform points in the world coordinate system can be accomplished by direct measurement, extracting the data from a FEM, or by using a coordinate measurement machine (CMM). For many test articles, particularly whose externals are relatively featureless, directly measuring point coordinates or extracting feature coordinates from a FEM accurately can be difficult. For example, in a recent test a set of CCC markers were placed on the test object and their coordinates were measured by hand using a tape measure. Using the LSRM transformation, the maximum, minimum and mean re-projection errors for the marker transform points were calculated and are shown in Table 1. To reduce this error, a FARO ScanArm CMM was used to more accurately measure the CCC marker locations in the world coordinate system. Using the LSRM transformation on the same example data set, the average re-projection error was reduced approximately 42%. With the rotation matrix and translation vector that transforms from the camera rig CS to the world, $[\mathbf{R}|t]_{\text{rig}\rightarrow\text{world}}$, established, the time history displacements can be converted to the world coordinate system using equation (1). When transforming geometry coordinates, the translation vector is utilized, whereas displacements (which are relative) will use a translation vector of $\mathbf{0}$.

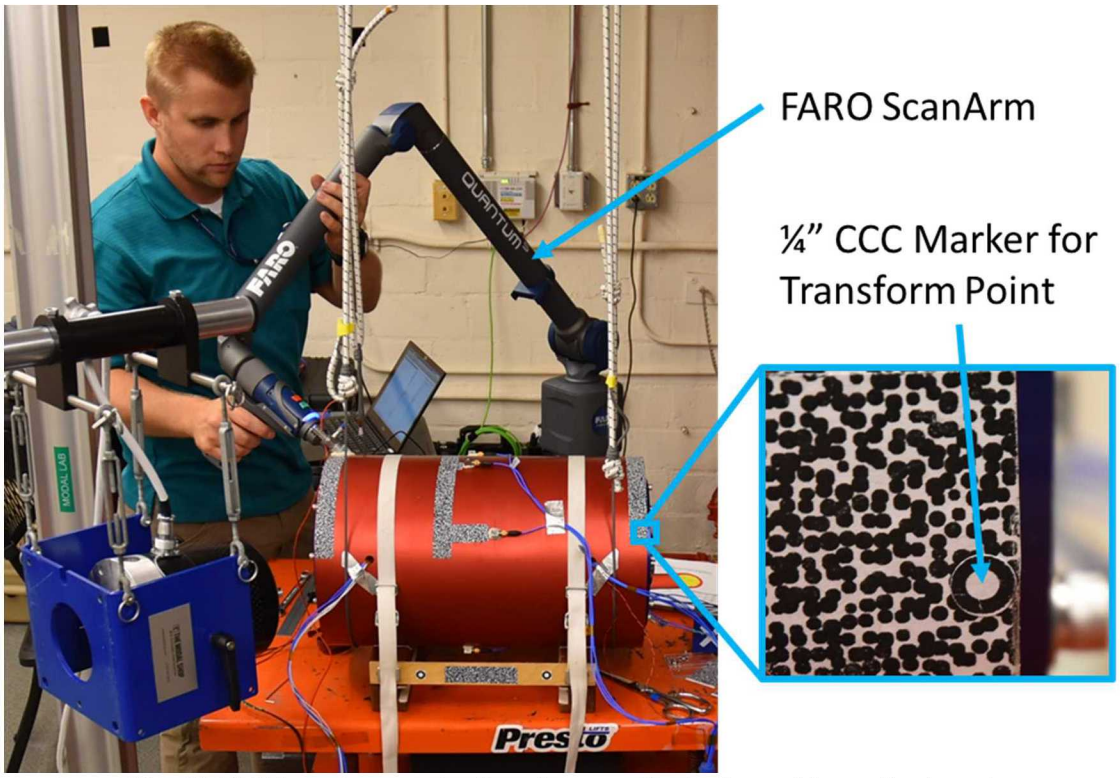

Fig. 10 CMM measurements of marker coordinates in world coordinate system

Table 1. Transform point re-projection errors

Error Measurements	Hand Measured (mm)	CMM Measured (mm)	Error Reduction (%)
Maximum	3.5	2.2	37%
Minimum	1.7	0.9	47%
Mean	2.4	1.4	42%

Two additional results from transforming the optical data to the world CS are (1) data sets from multiple camera views can easily be stitched together, allowing for full measurement coverage of a test object and (2) the subset test geometry coordinates can be directly recovered from their 3D coordinates of the reference image. This means the test geometry of the optically measured degrees of freedom (DOF) can be automatically generated and combined with any accelerometers, an example of which is shown in Fig. 11. The optically measured subset nodes are represented by the element object vertices, while the accelerometers are represented as individual nodes connected by trace lines.

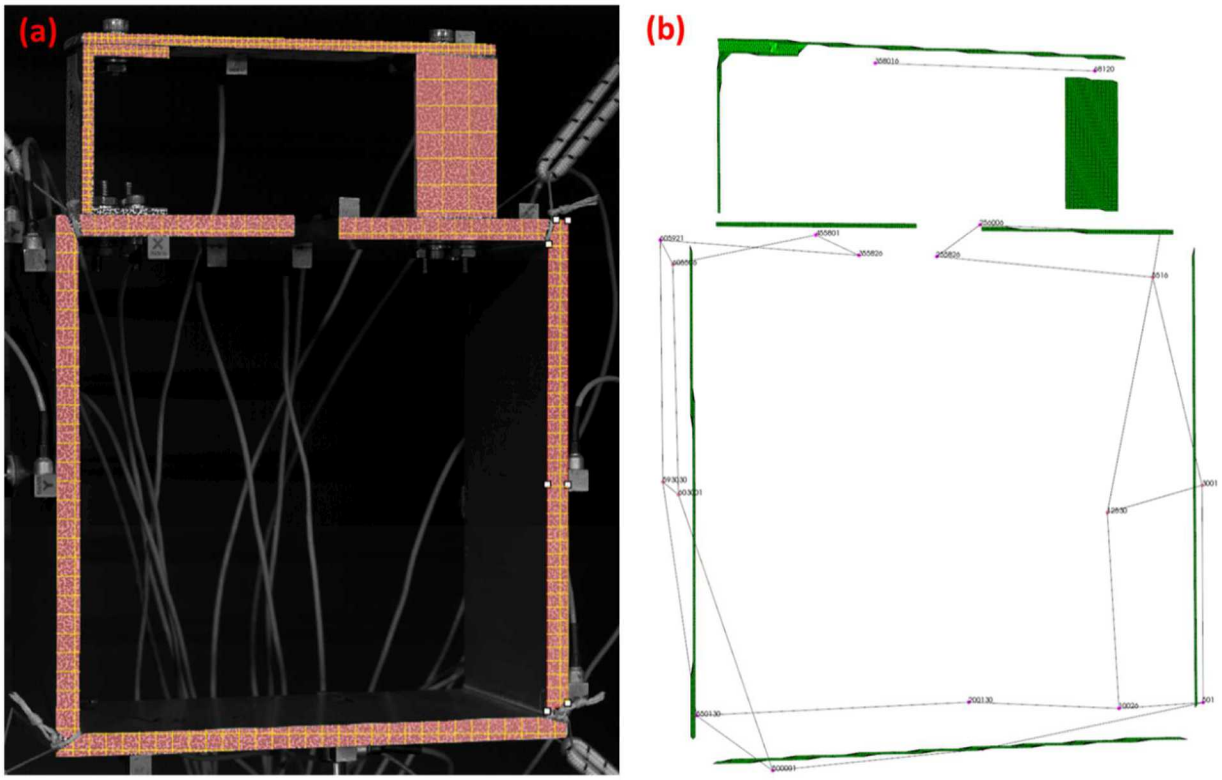

Fig. 11 Combined test geometry, (a) test image with scale-representative subsets and (b) combined test geometry (green elements represent DIC subset data, pink nodes on wireframe correspond to accelerometers)

With time history data in the correct coordinate system, a mean removal is performed. Next, acceleration time histories are calculated as the second derivative of the time history displacement data. The computation is performed in the frequency domain. Note that frequency domain derivative calculations are valid as long as the discrete Fourier transform (DFT) requirements are met to prevent leakage. Practically speaking, for random data, windowing is necessary to prevent end-effects in the final acceleration time histories.

Next, the accelerometer and load cell data recorded by the DAS are resampled to match the camera data if they are different. As mentioned above in the Section 3, care must be taken to avoid aliasing in the decimation process. This allows all data to be processed together at the same time, using the same post-processing parameters and methods.

To this point, the node identification numbers (IDs) of the optical subsets have been taken as the subset number from the DIC analysis. Unless otherwise specified by the user during DIC analysis, these subset node IDs will need to be appropriately offset to avoid naming conflicts with those of the accelerometers. Once this is completed the data sets from the DAS and DIC can be combined into one file that is ready for modal post-processing. Obviously, this file must be compatible with the modal parameter estimation software that will be used. FRFs are calculated per normal modal practice [16] between the input force and each output response measurement (accelerations from subsets and accelerometers) with the H1 estimator being the natural choice, given the level of noise expected in the subset response data.

The final step before modes can be extracted is to correct for the time delay present between the DAS and the cameras that was discussed in Section 3. The time delay is an unknown fraction of a time step which manifests as a drift in the phase angle of the FRFs, as seen in Fig. 12 (a). In addition to the phase angle drift that increases with frequency, the real and imaginary parts of the accelerance FRFs will appear to be switched, as shown in Fig. 13. The method chosen for phase angle correction is to fit a straight line though a user selected region of the FRFs phase angle data (where the drift is observable) using the Random Sample and Consensus (RANSAC) algorithm [12]. The linear slope and offset present in the data are established and used to calculate a correction term at each frequency line which is subsequently removed from the measured phase data. A corrected set of FRFs are then generated by recombining the magnitude with the corrected phase at each frequency line.

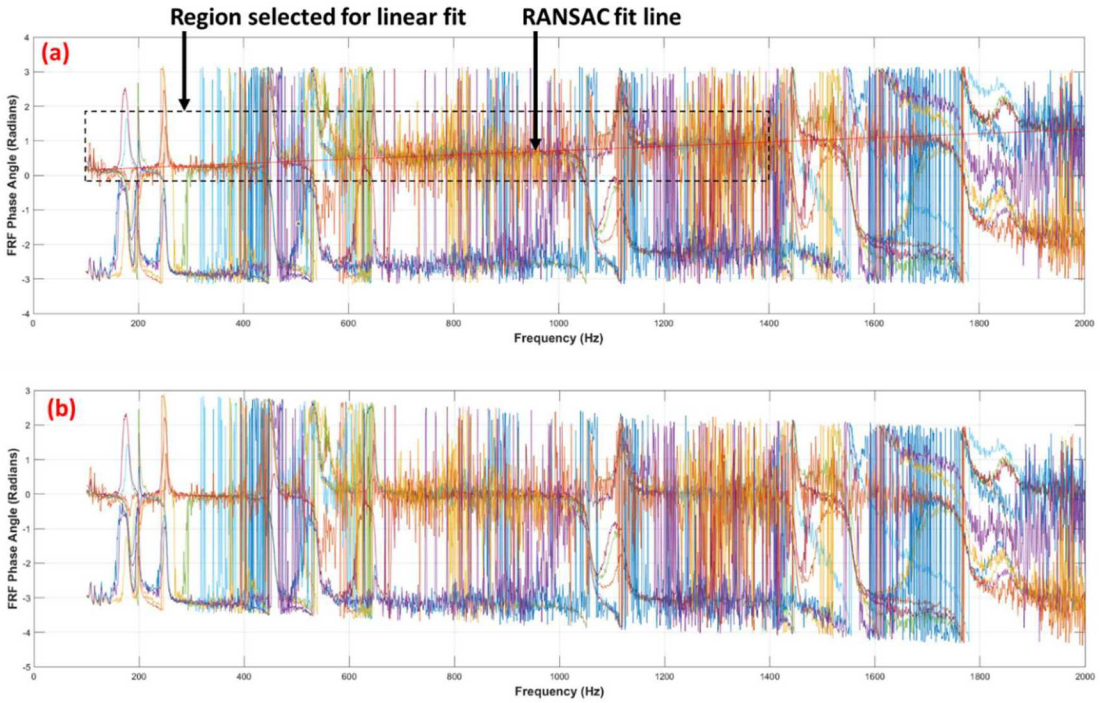

Fig. 12 FRF phase angle drift due to time delay, (a) uncorrected and (b) corrected by linear trend removal

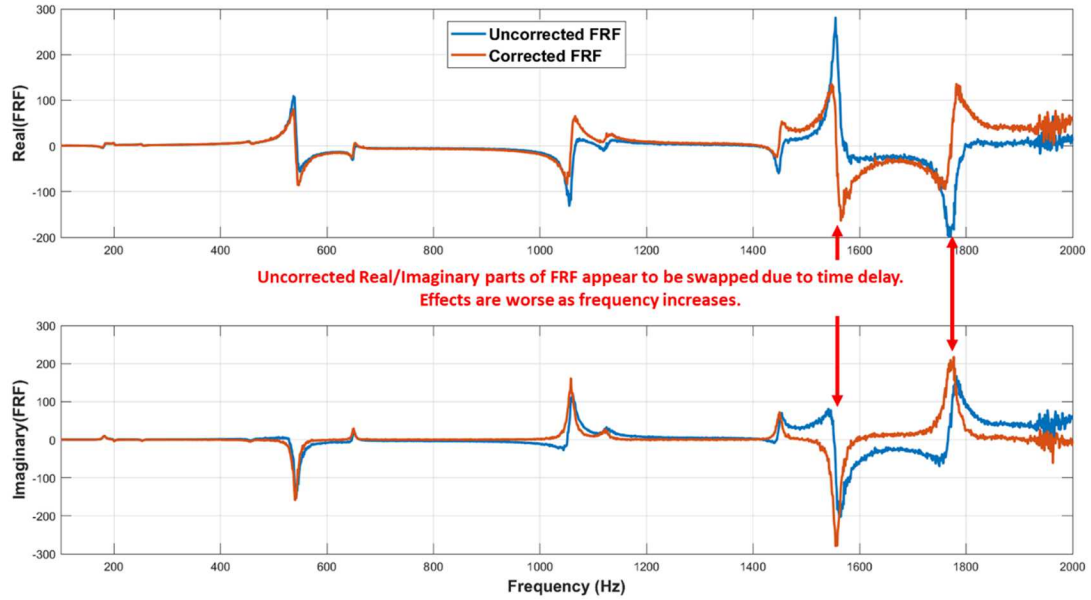

Fig. 13 Example accelerance FRF real/imaginary swapping due to time delay, (a) uncorrected and (b) corrected by linear trend removal

Once the time delay is accounted for, the data are sent to the modal parameter estimation algorithm of choice. Examples of mode shapes extracted from an academic test article are shown in Fig. 14. The process above was utilized with 10 averages of flat-force pseudorandom excitation, which were averaged in the image space prior to DIC analysis. The peak displacement across all subsets was calculated to be 0.3 pixels and modes were fit through 2000 Hz.

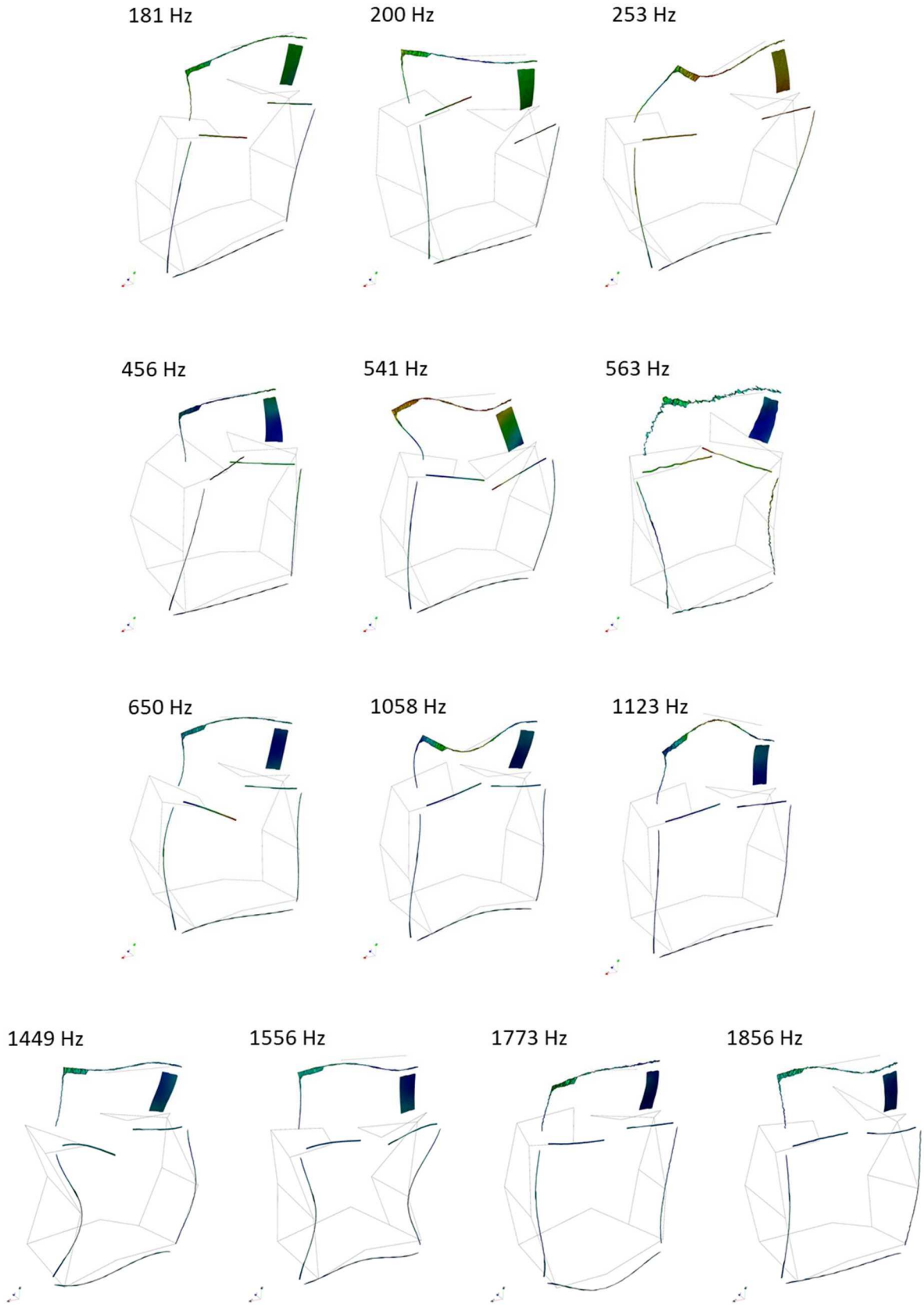

Fig. 14 Examples of low-amplitude, high-frequency (up to 1.8kHz) mode shapes extracted using DIC

5.2 Noise Mitigation

To this point, the only noise mitigation techniques employed were to ensure high contrast speckle patterns, increasing the number of pixels across the AOI, utilizing image (or frequency domain) averaging, and using an excitation method that excites higher frequency modes. As mentioned above, the use of larger subsets can help increase the signal-to-noise ratio but at the expense of spatial resolution and potential issues with pattern induced bias and shape function under-matching. The two former issues can be overcome by performing AOI averaging, where subsets within an AOI are averaged in the time domain. This works as a spatiotemporal filter at the cost of decreased spatial resolution, which is likely not an issue for modal applications. As an example, the test object shown in Fig. 8 had multiple AOI defined at locations where measurements were desired (red patches shown at the top of the figure). Within each AOI, an average of approximately 200 subsets were solved. All subsets for a given AOI were averaged together, and the averaged time history was assigned to the subset coordinates closest to the geometric center of the subset, resulting in the test geometry shown in the three sub-figures.

Another highly effective noise mitigation strategy for modal analysis to use the System Equivalent Reduction/Expansion (SEREP) [13]. Model reduction and expansion techniques are based on developing a transformation matrix, $\boldsymbol{T}$, that maps between a reduced space model (a-space, i.e. experimental degrees of freedom) and a full space (n-space) model. Methods such as Guyan [14] and Dynamic Condensation [15], for example, use system mass and stiffness matrices to form the transformation matrix. SEREP however uses a set of FEM mode shapes as the basis for the transformation matrix which allows for exact preservation of the mode shapes and frequencies, as well as the ability to arbitrarily select which modes and DOF to include in the reduction/expansion. The analytical mode shapes of a FEM in full n-space are denoted by $\boldsymbol{\Phi}_n$, whereas the same shapes at a reduced set of a DOF (measured DOF) are denoted by $\boldsymbol{\Phi}_a$. The SEREP transformation between full and reduced space mode shapes is then:

$$\boldsymbol{T} = \boldsymbol{\Phi}_n \boldsymbol{\Phi}_a^{\dagger} \tag{2}$$

where † indicates a generalized inverse. Experimental mode shapes, $\boldsymbol{\Psi}$, measured at a DOF can be expanded to the full FEM n-space DOF by:

$$\boldsymbol{\Psi}_n = \boldsymbol{T}\boldsymbol{\Psi}_a = \boldsymbol{\Phi}_n \boldsymbol{\Phi}_a^{\dagger} \boldsymbol{\Psi}_a \tag{3}$$

This method is not without limitations and caveats in usage. While the FEM used does not need to be exactly correlated to the test data, it is imperative that the FEM shapes span the space of the experimental shapes for an accurate expansion. For this reason, analytical rigid body mode shapes must be retained. Also, to prevent $\boldsymbol{\Psi}_n$ from being rank deficient, the number of DOF kept needs to be greater than or equal to the number of preserved modes ($a \geq m$). This is not an issue for a DIC based modal test which will almost assuredly have many more measured a DOF than extracted modes. This results in a least-squares approximation of the expanded $\boldsymbol{\Psi}_n$ and is precisely the reason that it serves so well as a noise mitigation strategy for optically measured shapes. The experimental shapes $\boldsymbol{\Psi}_a$ are projected through the FEM shapes via $\boldsymbol{\Phi}_n \boldsymbol{\Phi}_a^{\dagger}$, meaning only combinations of the FEM shapes can be used to create $\boldsymbol{\Psi}_n$. Since noise is not present in the FEM shapes, the noise in the experimental shapes is effectively removed in the projection. Care must be taken that an appropriate number of FEM shapes are included; inclusion of higher order shapes of the FEM could eventually allow noise to be projected also. The same least-squares smoothing can also be achieved in the measured DOF a-space as well by:

$$\boldsymbol{\Psi}_a' = \boldsymbol{\Phi}_a \boldsymbol{\Phi}_a^{\dagger} \boldsymbol{\Psi}_a \tag{4}$$

where $\boldsymbol{\Psi}_a'$ denotes the smoothed experimental shapes in the measurement a-space. Again, note that a must be greater than the number of modes included from the FEM for any smoothing to occur. An example of a noisy mode shape (mode 6 in Fig. 14) before and after SEREP smoothing/expansion are depicted in Fig. 15.

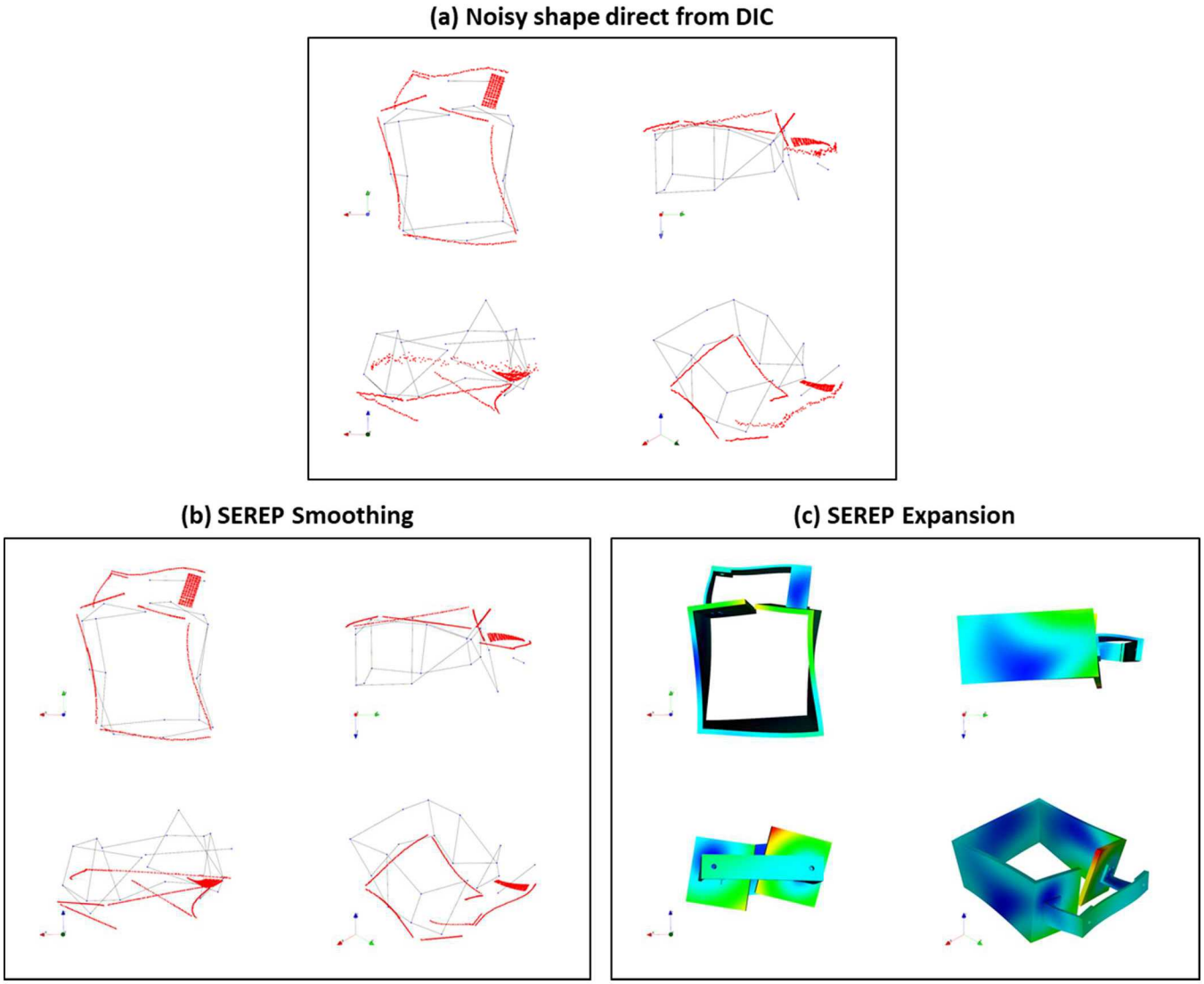

Fig. 15 Example of mode shape noise mitigation (a) raw, (b) SEREP smoothing and (c) SEREP expansion

6 CONCLUSIONS AND FUTURE WORK

Several practical aspects of performing an experimental modal analysis test using DIC have been presented, spanning the test planning, setup, execution and post-processing phases. The methods presented are by no means the only manner in which DIC could be used for modal testing and are offered as a starting point for anyone attempting to establish a similar dynamic measurement capability using photogrammetry.

The noise floor of the optical data acquisition system is easily identified as the primary limiting factor for EMA applications, followed closely by the data processing times that prevent “quick-look” troubleshooting that modal practitioners often rely on during testing. The first issue can be mitigated through proper test setup, object excitation, and post-processing techniques such as SEREP smoothing. Accordingly, a majority of the planned future work centers around novel ways to mitigate noise in optically measured data. Methods planned for future investigation include further test setup optimizations, Weiner filtering, and machine learning. Future work will also include examination of different pattern application materials and methods, including projected speckles, and their suitability for DIC modal testing.

7 REFERENCES

1 M. Helfrick, C. Niezrecki, P. Avitabile, T. Schmidt, "3D digital image correlation methods for full-field vibration measurement," Mechanical Systems and Signal Processing, Vol 25, pp. 917-927, 2011.

2 A. Molina-Viedma, E. Lopez-Alba, L. Felipe-Sese, F. Diaz, "Full-field modal analysis during base motion excitation using high-speed 3D digital image correlation," Measurment Science and Technology, Vol. 28, 2017.

3 E. Di Lorenzo *et al*, "Full-field modal analysis using high-speed 3D digital image correlation," Journal of Physics: Conference Series, 1149-012007, 2018.

4 "A Good Practices Guide for Digital Image Correlation," International Digital Image Correlation Society, E. Jones and M. Iadicola (Editors), 2018.

5 J. Javh, J. Slavic, M. Boltezar, "High Frequency Modal Identification on Noisy High-Speed Camera Data," Mechanical Systems and Signal Processing, Vol 98, pp. 344-351, 2018.

6 D. Rohe, "An Optical Test Simulator Based on the Open-Source Blender Software," Proceedings of the 38th International Modal Analysis Conference, Houston, TX, 2020.

7 A. Phillips, R. Allemang, "An Overview of MIMO-FRF Excitation/Averaging/Processing Techniques," Journal of Sound and Vibration, Vol 262, pp. 651-675, 2003.

8 C. Shih, Y. Tsuei, R. Allemang, D. Brown, "Complex Mode Indicator Function and its Applications to Spatial Domain Parameter Estimation," Mechanical Systems and Signal Processing, Vol 2, pp. 367-377, 1988.

9 M. Sutton, J. Orteu, H. Schreier, "Image Correlation for Shape, Motin and Deformation Measurements: Basic Concepts, Theory and Applications," Springer, 2009.

10 K. Arun, T. Huang, S. Blostein, "Least-Squares Fitting of Two 3-D Point Sets", IEEE Transactions on Pattern Analysis and Machine Intelligence, Vol PAMI-9, No 5, 1987.

11 D. Ewins, "Modal Testing, Theory, Practice and Applications," 2nd Edition, Research Studies Press, Baldock, UK, 2000.

12 M. Fischler, R. Bolles, "Random Sample Consensus: A Paradigm for Model Fitting with Applications to Image Analysis and Automated Cartography," Communications of the ACM, Vol 24, pp. 381-395, 1981.

13 J. O'Callahan, P. Avitabile, R. Riemer, "System Equivalent Reduction Expansion Process", 7th International Modal Analysis Conference, Las Vegas, Nevada, February 1989.

14 R. Guyan, "Reduction of Stiffness and Mass Matrices", AIAA Journal, Vol 3, No 2, 1965.

15 R. Kidder, "Reduction of Structure Frequency Equations", AIAA Journal, Vol 11, No 6, 1973.